Semicond. Sci. Technol. **11** (1996) 308–314. Printed in the UK

The role of randomly distributed well widths in disordered GaAs/AlGaAs superlattices

G F Lorusso†, V Capozzi‡, J L Staehli†, C Flesia§, D Martin‖, P Favia¶ and G Perna‡

† Institut de Physique Appliquée, Ecole Politecnique Fédérale de Lausanne, CH-1015 Lausanne, Switzerland
‡ Dipartimento di Fisica dell' Universitá di Bari, and Istituto Nazionale di Fisica delle Materia, Unitá di Bari, Via Amendola, 173, I-70126 Bari, Italy
§ Groupe de Physique Appliquée, Université de Geneve, CH-1211 Geneve 4, Switzerland
‖ Institut de Micro- et Optoélectronique, Ecole Politecnique Fédérale de Lausanne, CH-1015 Lausanne, Switzerland
¶ Institut de Génie Atomique, Ecole Politecnique Fédérale de Lausanne, CH-1015 Lausanne, Switzerland

Received 17 October 1995, accepted for publication 18 December 1995

Abstract. Numerical and experimental results on the effect of randomness in $GaAs/Al_{0.3}Ga_{0.7}As$ superlattices having a small number of randomly distributed well widths are reported. The numerical results indicate the splitting of the extended state miniband into sub-minibands of localized states having a disorder-induced fine structure. The comparison between the experimental results for low-temperature absorption spectra and the computed joint density of states of the investigated samples confirms the predicted features. The high-temperature photoluminescence intensity of random superlattices is observed to be enhanced with respect to the ordered case.

1. Introduction

Disordered superlattices (d-SLs) are considered to be one of the most powerful tools to investigate Anderson localization [1] and transitions between localized and extended states [2]. Theoretical calculations on the effects of disorder on superlattice (SL) properties [3, 4] strongly stimulated experimental investigations on d-SLs [5–8], and, in particular, d-SLs with Gaussian distributed well widths were widely used to investigate the disorder-induced localization of carriers [5–8]. Furthermore, the localization of carriers in semiconductor materials has attracted a growing interest in recent years [9, 10]. It was reported that the disorder-induced localization of carriers enhances the electron–hole transition rate [9], similarly to the confinement of carriers in a single quantum well (SQW) [11], where the recombination efficiency increases as the well width is lowered. In consequence, the photoluminescence (PL) and the electroluminescence (EL) efficiency of d-SLs are larger than those of the bulk material and of ordered SLs (o-SLs) [9, 10]. Such a result indicated that the study of d-SLs with tailored properties could be usefully exploited in the fabrication of optoelectronic devices [9] and could contribute to the understanding of quantum-confinement-induced effects.

The technological interest in the study of d-SLs stimulated new theoretical efforts [12–16] devoted to predict electronic and optical properties of d-SLs. A significant dependence of the localization degree on the random sequence of the d-SL was evidenced [14]. The study of one-dimensional (1D) d-SLs within the framework of the effective mass approximation in the Wannier–Bloch mixing representation [12, 13] accounted for the observed redshift of the absorption edge [9] and predicted that the features of optical absorption spectra of d-SLs should become richer as the disorder is increased [12]. It indicated also that the mixing of the heavy-hole (HH) and light-hole (LH) subbands results in a large nonparabolicity, which will produce some weak structures corresponding to forbidden transitions in SQWs [13]. Furthermore, the study of d-SLs using realistic pseudopotentials [15, 16] evidenced the formation of disorder-induced impurity-like states, as well as the transition from indirect to direct bandgap material of short-period d-SLs.

In this work we discuss numerical and experimental results on the effect of randomness in $GaAs/Al_xGa_{1-x}As$ SLs ($x = 0.3$) having randomly distributed well widths. A wider disorder range with respect to previous studies is investigated. In section 2 we describe how the disorder is introduced in the SLs. The numerical methods [17–20]

0268-1242/96/030308+07$19.50

are summarized in section 3.1, and the numerical results for the density of states (DOS) and for the joint density of states (JDOS) of the investigated samples are discussed in section 3.2. The experimental methods are reported in section 4.1, and in section 4.2 we discuss the experimental results of the low-temperature absorption spectra and the temperature dependence of the PL intensity. Section 5 contains the concluding remarks.

2. The model for disordered superlattices

In the d-SLs considered here the thickness L of every layer is a random variable with probability distribution $P(L)$. In particular, we investigate d-SLs having constant barrier thickness L_B. L_{Wi} ($i \in \{1, \ldots, N_W\}$) are the possible values of the well thickness in the d-SLs. N_W is the number of different well widths present in the d-SLs and i is an integer stochastic variable. L_{Wi} is measured in atomic monolayer (ML) units. The degree of disorder in the SLs can be varied as follows. We considered a class of d-SLs where the well thicknesses L_{Wi} are expressed by the following relationships:

$$L_{Wi} = L_{Wmin} + (i-1)\Delta L_W \qquad i \in \{1, \ldots, N_W\}. \quad (1)$$

Here, L_{Wmin} is the minimum well width in the d-SLs and ΔL_W is a parameter permitting us to change the degree of disorder in the SL. In this work we investigate a simple class of d-SLs having four different well thicknesses ($N_W = 4$) and different degrees of disorder, as shown in figure 1. When $\Delta L_W \to 0$, an ordered sequence of layers is achieved, and the degree of disorder is zero. When ΔL_W is increased, the difference between the minimum and the maximum well thickness in the d-SLs is increased and the width of the distribution of the energy in the SL sites is larger, thus increasing the degree of disorder according the Anderson definition [1].

3. Numerical analysis

3.1. Numerical methods

The matrix propagation technique [17–20] has been used in order to calculate the electron (e), light hole (LH) and heavy hole (HH) densities of states and Lyapunov exponent in d-SLs. The carrier wavefunction ψ in the lth layer will depend on the coefficients A_l and B_l, representing the amplitudes of the waves propagating in opposite directions. The transfer matrix $\mathcal{T}_{l\to l+1}$ which joins the wavefunction coefficients of the lth layer with those of the $(l+1)$th layer is defined by

$$\begin{pmatrix} A_{l+1} \\ B_{l+1} \end{pmatrix} = \mathcal{T}_{l\to l+1} \begin{pmatrix} A_l \\ B_l \end{pmatrix}. \quad (2)$$

$\mathcal{T}_{l\to l+1}$ can be obtained by using the particle current-conserving boundary conditions, i.e. by requiring that ψ and $(1/m(z))(\mathrm{d}\psi/\mathrm{d}z)$ are continuous at each interface. Here $m(z)$ is the carrier effective mass. The transfer matrix method allows us to get information on the localization of the states by computing the Lyapunov exponent $\gamma(E)$,

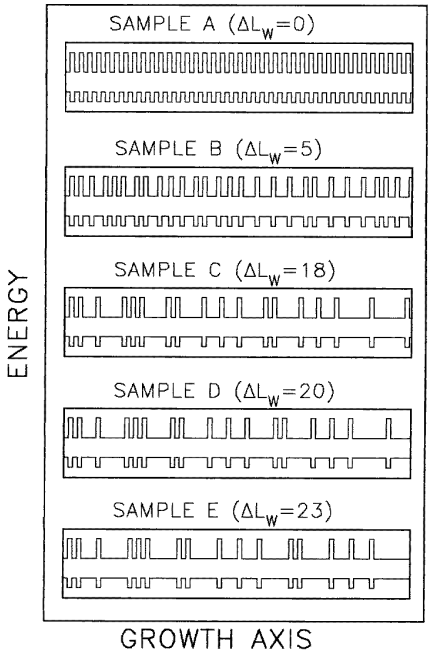

Figure 1. A portion of a schematic potential profile of the five investigated samples. The disorder increases from sample A to sample E.

which is proportional to the reciprocal of the mean localization length $\lambda(E)$ of states [21]. In the case of localized states the amplitude of the wavefunction near some point z_o in which it has a maximum will on average decay as [21]

$$\overline{|\Psi(|z-z_o|, E)|} \simeq \exp[-|z-z_o|\gamma(E)]. \quad (3)$$

Here the overline indicates the average behaviour of the probability amplitude in the SL. Furthermore, the transfer matrix method permits the calculation of the integrated density of states $D(E)$, which is related to the 1D DOS $\rho(E)$ by [17]

$$D(E) = \int_0^E \rho(E')\,\mathrm{d}E'. \quad (4)$$

The integrated DOS $D(E)$ is proportional to the three-dimensional (3D) DOS in the material. In our calculations we used the following material parameters [22]: bandgap $E_g = (1.5194 + 1.48x)$ eV, electron effective mass $m_e = (0.0665 + 0.0835x)m_0$, HH effective mass $m_{HH} = (0.51 + 0.20x)m_0$ and LH effective mass $m_{LH} = (0.082 + 0.078x)m_0$, where m_0 is the free electron mass. A band-offset ratio of $\Delta E_c/\Delta E_v = 0.65/0.35$ is used, corresponding to a conduction (valence) band discontinuity of 288 meV (155 meV) between GaAs and $Al_{0.3}Ga_{0.7}As$ [23].

3.2. Numerical results

The integrated electron densities of states $D(E)$ predicted by the transfer matrix method for electrons in a d-SL and in an o-SL are compared in figure 2. Similar behaviour

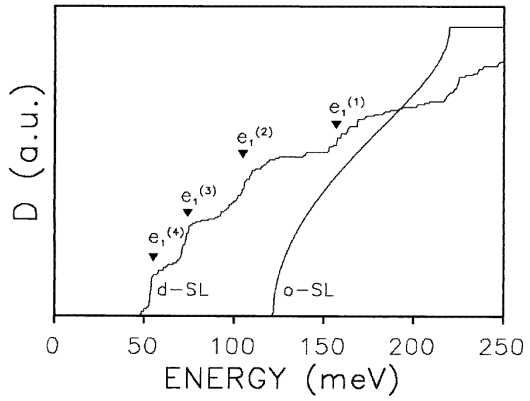

Figure 2. The integrated electron density of states $D(E)$ of a d-SL with randomly distributed well widths and of an o-SL. The disorder causes the splitting of the nth miniband into sub-minibands centred on the SQW eigenenergies $e_n^{(i)}$, corresponding to the different well thicknesses L_{Wi} present in the d-SL. The resolution is 0.5 meV.

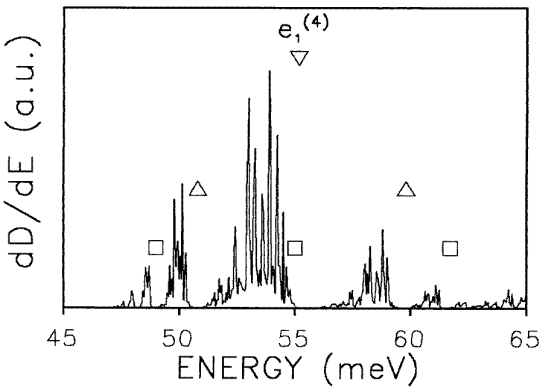

Figure 3. The disorder-induced fine structure of one of the sub-minibands of localized states shown in figure 2. The symbols indicate eigenenergies of single (▽), double (△) and triple (□) QWs. The resolution is 0.05 meV.

was observed for HHs and LHs. The d-SL investigated in figure 2 has $\Delta L_W = 5$, with four different kinds of well ($N_W = 4$) having the same probability of occurrence ($P(L_{Wi}) = \frac{1}{4}\ \forall i \in \{1, \ldots, 4\}$), and with $L_{Wmin} = L_B = 9$ ML. The o-SL has $L_W = L_B = 9$ ML. The splitting of the electron miniband into four different sub-minibands of states is evident in the $D(E)$ of the d-SLs. This splitting has already been observed [7] for the HH miniband only, but not yet for the LH and e minibands. The sub-minibands are centred on the eigenvalues of energy $e_n^{(i)}$ of SQWs of widths L_{Wi} (triangles in figure 2). The eigenenergies $e_n^{(i)}$ have been computed by means of the transfer matrix method. Furthermore, the computed Lyapunov exponents indicated that the states in the d-SL sub-minibands are more or less localized ($\gamma(E) > 0$), while the states in the o-SL miniband are extended ($\gamma(E) = 0$). It is then quite natural to assume that the carriers with energy $e_n^{(i)}$ are essentially localized in the wells of width L_{Wi}. The Lyapunov exponents also indicated that the localization of the carriers near the band edge increases as the disorder parameter ΔL_W is increased.

Figure 3 shows the 1D electron DOS $\rho(E)$ of one of the sub-minibands present in figure 2. The d-SL sub-miniband of localized states shows a considerable amount of fine structure, indicated by the presence of states at lower and higher energies with respect to the SQW eigenvalue. This is a novel result in the investigation of d-SLs, although similar disorder-induced fine structures have been reported in numerical works on 1D disordered systems [24] and in experimental results on layered disordered semiconductors [25]. Our simulations indicated that the disorder-induced fine structure is mainly related to the coupling between wells having the same width, which causes new allowed states at lower and higher energies with respect to the SQW case. In fact, the eigenenergies of single, double and triple QW calculated by means of the transfer matrix method (symbols in figure 3) correspond to the main features of the disorder-induced fine structure. An even more accurate agreement can be obtained by also considering the coupling between wells having different well widths.

The evolution of the electron miniband of states as a function of the disorder parameter ΔL_W for the investigated class of d-SLs is reported in figure 4. As already observed in figures 2 and 3, the main effects of the disorder are: (i) the splitting of the extended state miniband into sub-minibands, and (ii) the disorder-induced fine structure of the sub-minibands. These two effects are quite general, i.e. they were not found to be related to the particular kind of disorder investigated here. Furthermore, a sub-miniband narrowing with ΔL_W is observed because the coupling between the fundamental levels of wells is reduced with increasing well widths. In consequence, the disorder-induced fine structure is better evidenced for small values of the disorder parameter ΔL_W, for which the sub-minibands of localized states can be easily resolved.

Quantitative information about the absorption spectra of the investigated d-SLs can be obtained by computing the JDOS. The localization of the sub-miniband states mentioned above indicates that the optical transitions in d-SLs will mainly occur between energetic states of the same well, thus suggesting that a multiple quantum well (MQW) model of recombination in d-SLs should account for the main features of the optical absorption spectra: transitions between electron and hole states localized in different wells will then be considered as improbable in the following. The absorption coefficient for interband transitions can be written, neglecting excitonic effects, as [12]

$$\alpha(\hbar w) = (\hbar w)^{-1} \sum_{n_i, n_i'} |P_{n_i, n_i'}|^2 D_{n_i, n_i'}(\hbar w). \qquad (5)$$

As before, $i \in \{1, \ldots, N_W\}$ denotes the sub-minibands belonging to L_{Wi}. $P_{n_i, n_i'}$ denotes the momentum matrix element and $D_{n,n'}$ is the JDOS between the eigenstate of the n_ith conduction sub-miniband with energy E_n and the eigenstate of the n_i'th valence sub-miniband with energy $E_{n'}$. Only the contributions from electron–hole pair states with a total wavevector $k_\parallel = 0$ and $\Delta n = 0$ are taken into account [12].

The 1D JDOS $\rho_{n_i, n_i'}(\hbar w) \propto \mathrm{d}D_{n_i, n_i'}(\hbar w)/\mathrm{d}(\hbar w)$ for the four investigated samples are shown in figure 5, which shows a redshift of the JDOS absorption edge as

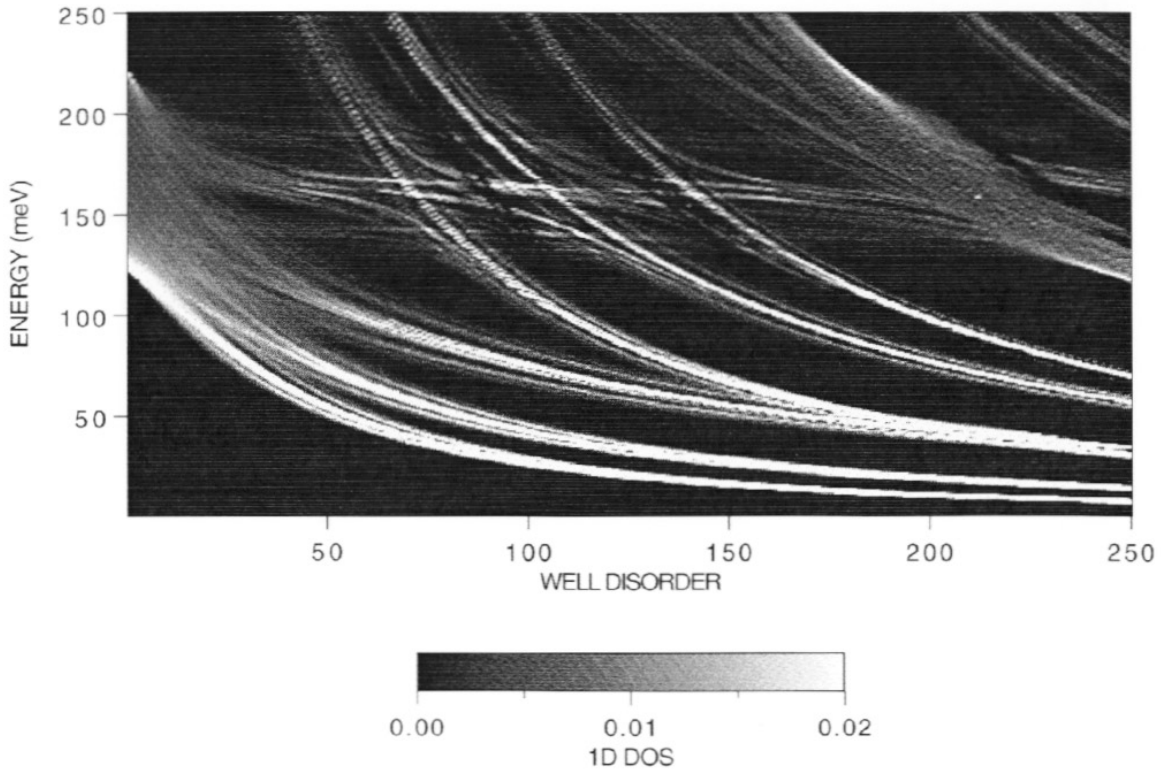

Figure 4. The evolution of the electron miniband of states as a function of the disorder parameter ΔL_W for the investigated class of d-SLs. The grey scale indicates the 1D DOS. The splitting into sub-minibands as well as the disorder-induced fine structure are clearly evident. The resolution is 1 meV.

the disorder parameter ΔL_W is increased. Furthermore, the disorder-induced fine structure is most evident in the sample having the smaller values of ΔL_W (sample B). We remark that 1D JDOS are reported in order to have an easier comparison with experimental results, where excitonic peaks are present. In fact, in our theoretical calculations excitonic effects have been neglected. Thus the 3D JDOS obtained in this approximation is expected to be a series of steps. To make a comparison between our approximate theoretical results and the measured optical transmission spectra easier, we report the 1D JDOS, i.e. a series of peaks whose amplitudes are proportional to the step heights, and thus approximate the exciton oscillator strengths. Therefore, we compare here only the calculated spectral positions of the peaks, and their relative heights, with those observed in the absorption spectra. We do not pretend to compare lineshapes, which would be completely inadequate.

4. Experimental analysis

4.1. Experimental methods

The SL structures were grown by means of molecular beam epitaxy (MBE) at a temperature T of 620 °C on (001)-oriented GaAs substrates. They consist of a GaAs substrate upon which there are a buffer layer of GaAs (0.3 μm thick), the GaAs/$Al_{0.3}Ga_{0.7}As$ SL (1 μm thick) cladded between two $Al_{0.3}Ga_{0.7}As$ layers (each 1 μm thick) and a GaAs cap-layer (20 nm). The growth rates were 0.6 μm h^{-1}. The ordered SL nominally contains 9/9 monolayers of GaAs/$Al_{0.3}Ga_{0.7}As$ and has 200 periods. The error on the layer thickness is about 1 ML. The samples were prepared for transmission electron microscopy (TEM) by means of a wedge cleaving technique. TEM was carried out at 300 keV, with a resolution of 0.2 nm. In figure 6 we show a TEM micrograph of a d-SL. The complete TEM analysis consists of eight partially overlapping TEM micrographs for each sample. The Al concentration x of the barriers was deduced from the PL spectral position of the HH exciton line of the AlGaAs cladding layer at 2 K and was found to be $x = 0.30 \pm 0.01$ [26]. In order to perform optical transmission measurements, the GaAs substrate was etched away using a selective etching solution [27] on a region having a diameter of about 0.5 mm. The etched samples were anodized to avoid multiple reflections of light [28]. The samples were immersed in superfluid He at 2 K and illuminated by means of a tungsten filament lamp. The light propagated along the growth axis of the samples and the illuminated spot was of about 50 μm diameter. The transmitted light was analysed with a double spectrometer (resolution of about 1 meV) and detected by means of a cooled GaAs photomultiplier tube. The spectra were recorded by using standard lock-in techniques. For the PL measurements, the samples were put in an He closed-cycle cryostat, whose temperature could be varied from 8 to 300 K within 0.5 K of uncertainty. The samples were photoexcited at $\pi/4$ using the 514 nm line of an Ar-ion

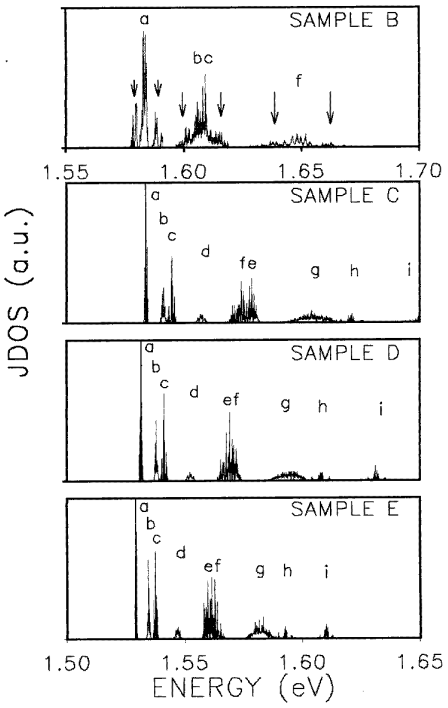

Figure 5. The computed 1D JDOS for the four investigated d-SLs. A redshift of the absorption edge is evident as the disorder is increased and the disorder-induced fine structure is more pronounced in the sample with the smaller values of ΔL_W (arrows). The meanings of the labels are: a=e–$HH_1(4)$, b=e–$LH_1(4)$, c=e–$HH_1(3)$, d=e–$LH_1(3)$, e=e–$HH_2(4)$, f=e–$HH_1(2)$, g=e–$LH_1(2)$, h=e–$HH_2(3)$ and i=e–$HH_2(2)$. Here e–$HH_n(i)$ and e–$LH_n(i)$ indicate respectively the transition between the e sub-miniband and the HH or LH sub-miniband with the same n in the same well of width L_{Wi}. The resolution is 0.1 meV.

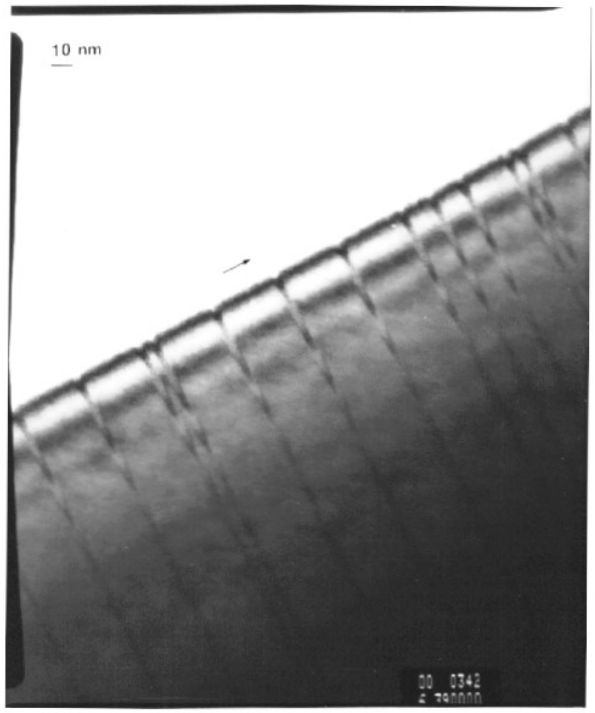

Figure 6. Transmission electron micrograph of a disordered superlattice (sample E). The arrow indicates the growth axis. The resolution is 0.2 nm.

laser, whose light beam was focused on a spot of about 100 μm diameter. The emission light was collected at $\pi/2$ with respect to the incident beam and was analysed by a double-grating spectrometer. The signal was detected by means of a cooled GaAs photomultiplier and was recorded using photon counting techniques.

4.2. Experimental results and discussion

In figure 7 we show the absorption spectra for the o-SL (sample A) and for the four d-SLs (samples B–E). In the ordered case, the absorption spectrum shows the well known features [23]: the two resolved peaks correspond to the ground state of the HH and LH ground state excitonic transitions, indicated as X_1^{HH} and X_1^{LH} respectively. The shoulder between the two peaks can be ascribed to the entire sequences of 2s, 3s, ... of HH excitonic transitions, superimposed on the absorption by excitonic scattering states; this is a further confirmation of the good sample quality. The absorption spectra of d-SLs show the redshift of the absorption edge evidenced by the numerical calculations. Moreover, the absorption spectra become richer in structures by increasing the disorder, as predicted [12]. The numerical results for the JDOS of d-SLs (figure 5) agree fairly well with the experimental features of the absorption spectra of d-SLs, thus confirming the validity of the MQW model of recombination in d-SLs, used in the calculation of the JDOS. Furthermore, the approximate numerical results reported in figure 5 permit us to identify most of the structures present in the experimental absorption spectra (labels in figure 7), thus giving a deeper insight into the optical properties of d-SLs. A few weak structures that are not predicted by our 1D MQW model (pulses in figure 7) could be ascribed to predicted HH–LH subband mixing [13] or to enhancement of the oscillator strength of interwell transitions related to Coulomb attraction.

In addition, the absorption spectra confirm the prediction of the numerical analysis on disorder-induced fine structure: in the limit of small disorder parameter ΔL_W, where the lines are relatively wide, several predicted shoulders and additional peaks appear (arrows in figure 7), while as the disorder parameter is increased the observed structures are quite narrow and the disorder-induced fine structure cannot be resolved. The disorder-induced fine structure was found to be in agreement with its numerical prediction (figure 5).

We note that the energies of the experimental absorption peaks are a few meV below the numerical predictions. This fact indicates that the observed optical features are excitonic transitions, and excitonic binding energies must be accounted for. An estimation of the excitonic binding energy in the investigated d-SLs is given by the difference between the predicted interband transition (figure 5) and the experimental excitonic recombination energies (figure 7). For small ΔL_W (sample B), the excitonic binding energies were found to be quite small with respect to the excitonic binding energies in MQWs [29], thus indicating a weak

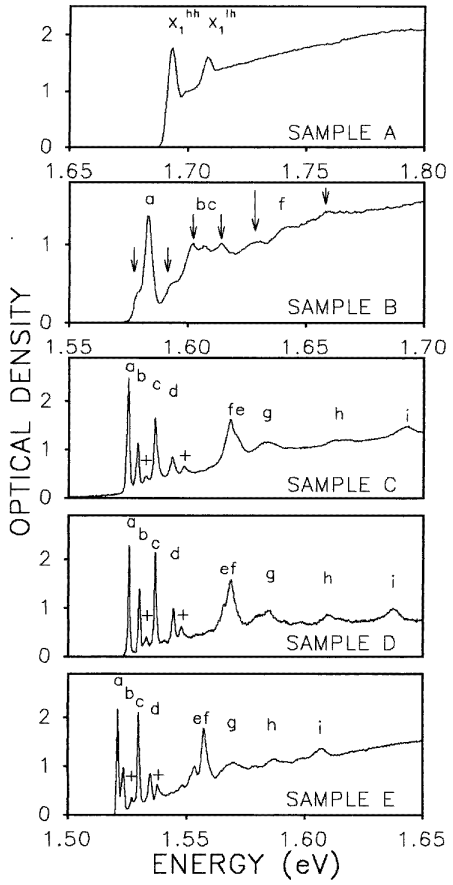

Figure 7. Absorption spectra for an o-SL (sample A) and d-SLs (samples B–E). The absorption spectra of d-SLs show the expected redshift of the absorption edge and the disorder-induced fine structure (arrows). The labels X_1^{HH} and X_1^{LH} indicate respectively HH and LH ground-state excitons. The labels from a to i have the same meaning as in figure 5. The resolution is about 1 meV.

localization of the carriers in this limit. In contrast, in the limit of large ΔL_W, the excitonic binding energies practically correspond to the Rydberg value in the MQW. Thus, the excitonic binding energies in a d-SL become more and more similar to the excitonic binding energy in MQWs as the disorder parameter ΔL_W is increased, as expected because of the increasing of the localization effects with ΔL_W. Furthermore, the enhancement of electron–hole Coulomb attraction could cause self-trapping of excitons in wider wells.

The temperature dependence of the integrated intensity of PL spectra of the o-SL and of the four discussed d-SLs are reported in figure 8. The PL-intensity of the o-SL is larger than those of the d-SLs at very low T, but it is strongly quenched as T increases. At $T = 100$ K the PL intensity of the o-SL is reduced by four orders of magnitude. The high-T PL intensity of the investigated d-SLs is much stronger than that of the o-SL: the PL intensity of d-SLs at room temperature is comparable to that of the o-SL at 100 K. This effect can be attributed to disorder-induced localization of excitons along the growth axis of samples. It prevents the motion of electron–hole

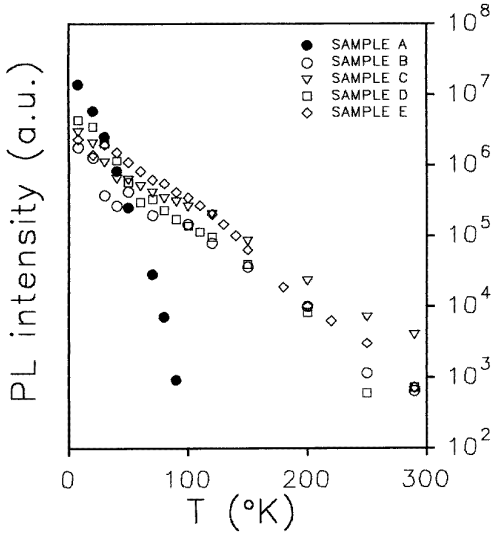

Figure 8. Temperature dependence of the integrated PL intensity for the o-SL (filled symbols) and d-SLs (open symbols). The high-temperature PL intensity of d-SLs is enhanced with respect to that of the o-SL.

pairs through the samples and reduces the non-radiative recombination probability. These PL results are promising for a possible device application of d-SLs.

5. Conclusion

In conclusion, our numerical and experimental results evidence the splitting of the miniband of extended states into sub-minibands of localized states having a disorder-induced fine structure. The numerical results permit us to identify most of the observed features in the experimental absorption spectra. The high-T PL intensity of the d-SLs was found to be enhanced with respect to the ordered case, thus confirming the attractive features of d-SLs for technological purposes.

Acknowledgments

We are grateful to A Minafra and F K Reinhart for their interest and encouragement in this work. This work was in part supported by the Consiglio Nazionale delle Ricerche, by the Istituto Nazionale di Fisica della Materia and by the Fonds National Suisse de la Recherche Scientifique.

References

[1] Anderson P W 1958 *Phys. Rev.* **109** 1492
[2] Lee P A and Ramacrishnan T V 1985 *Rev. Mod. Phys.* **57** 287
[3] Dow J D, Ren S Y and Hess K 1982 *Phys. Rev.* B **25** 6218
[4] Das Sarma S, Kobayashi A and Prange R E 1986 *Phys. Rev. Lett.* **56** 1280
[5] Chomette A, Deveaud B, Regreny A and Bastard G 1986 *Phys. Rev. Lett.* **57** 1464
[6] Tuncel E, Pavesi L, Martin D and Reinhart F K 1988 *Phys. Rev.* B **38** 1597

[7] Pavesi L, Tuncel E, Zimmermann B and Reinhart F K 1989 *Phys. Rev.* B **39** 7788
[8] Pavesi L and Reinhart F K 1990 *Phys. Rev.* B **42** 11 362
[9] Yamamoto T, Kasu M, Noda S and Sasaki A 1990 *J. Appl. Phys.* **68** 5318
[10] Sasaki M A, Wang X and Wakahara A 1994 *Appl. Phys. Lett.* **64** 2016
[11] Christen J, Bimberg D, Steckenborn A and Weimann G 1984 *Appl. Phys. Lett.* **44** 84
[12] Chen X and Xiong S 1993 *Phys. Rev.* B **47** 7146
[13] Chen X and Xiong S 1993 *Phys. Rev.* B **48** 5273
[14] Su W P and Shih H D 1992 *J. Appl. Phys.* **72** 2080
[15] Mäder K A, Wang L W and Zunger A 1995 *Phys. Rev. Lett.* **74** 13
[16] Mäder K A and Zunger A 1995 *Europhys. Lett.* **31** 107
[17] Ostlund S and Pandit R 1984 *Phys. Rev.* B **29** 1394
[18] Kohmoto M 1986 *Phys. Rev.* B **34** 5043
[19] Pavesi L and Reinhart F K 1990 *Phys. Status Solidi* b **157** 615
[20] Crisanti A, Flesia C, Pasquarello A and Vulpiani A 1989 *J. Phys. C: Condens. Matter* **1** 9509
[21] Halperin B I 1967 *Adv. Chem. Phys.* **13** 123
[22] Guzzi M and Staehli J L 1989 *Solid State Phenom.* **10** 22
[23] Capozzi V, Staehli J L, Flesia C, Martin D, Augelli V and Lorusso G F 1991 *Optics of Excitons in Confined Systems (Inst. Phys. Conf. Ser. 123)* (Bristol: Institute of Physics) p 195
[24] Gubernatis J E and Taylor P L 1973 *J. Phys. C: Solid State Phys.* **6** 1889
[25] Forney J J, Maschke K and Mooser E 1977 *J. Phys. C: Solid State Phys.* **10** 1887
[26] Bosio C, Staehli J L, Guzzi M, Burri G and Logan R A 1988 *Phys. Rev.* B **38** 3263
[27] LePore J J 1980 *J. Appl. Phys.* **51** 6441
[28] Yu J, Aoyagi Y, Iwai S, Toyoda K and Namba S 1984 *J. Appl. Phys.* **56** 1895
[29] Andreani L C and Pasquarello A 1990 *Phys. Rev.* B **42** 8928